A study on structural properties, conductivity and FT-IR spectroscopy of Cu–Al doubly substituted Bi4V2O11

Rachida Essalim, Abdelaziz Ammar, Mohamed Zamama, Fabrice Mauvy

A Study on Structural Properties, Conductivity and FT-IR Spectroscopy of Cu-Al Doubly Substituted $Bi_4V_2O_{11}$

R. Essalim[(a)], A. Ammar[(a)], M. Zamama[(b)] and F. Mauvy[(c)]

[(a)] Laboratoire des Sciences des Matériaux Inorganiques et leurs Applications (LASMIA), Equipe Matériaux à Faible Dimensionnalité (EMAFAD), Faculté des Sciences- Semlalia, Av. My Abdellah, B.P. 2390, Marrakech, Morocco.

[(b)] Laboratoire Physico-Chimie des Matériaux et Environnement (LPCME), Faculté des Sciences- Semlalia, Av. My Abdellah, B.P. 2390, Marrakech, Morocco.

[(c)] CNRS, Université de Bordeaux, (ICMCB), UMR 5026, 87, Av. Dr A. Schweitzer, 33608, Pessac, France

Abstract

The double-substituted solid solutions $Bi_4V_{2-x}Cu_{x/2}Al_{x/2}O_{11-5x/4}$, with identical quantitative compositions of Cu^{2+} and Al^{3+} ions, can occur for a substitution rate $0.1 \leq x \leq 0.6$. The compound with $x = 0.1$ is found to be a monoclinic α-form of $Bi_4V_2O_{11}$, whereas compounds with $0.2 \leq x \leq 0.6$ are found to be tetragonal γ and γ' polymorphs. We used electrochemical impedance spectroscopy to measure the electrical conductivity of doped samples in the temperature range of 250–700 °C. The slope changes observed in the Arrhenius plots might be related to the microstructural transitions occurring in these compounds. The sample with $x = 0.2$ shows the highest ionic conductivity values.

Keywords: Bismuth vanadium oxide; BIMEVOX materials; Ionic conductors.

1. Introduction

The structure of $Bi_4V_2O_{11}$ with intrinsic oxygen vacancies can be described as an intergrowth of the fluorite-type $(Bi_2O_2)^{2+}$ layers and oxygen-deficient perovskite-like $(VO_{3.5}\square_{0.5})^{2-}$sheets **[1].** This compound exists in three thermodynamically stable crystallographic polymorphs depending on disorder in oxygen vacancies. The low-temperature orthorhombic form α-$Bi_4V_2O_{11}$ changes into the orthorhombic β- $Bi_4V_2O_{11}$ at 450°C, then into the tetragonal γ-$Bi_4V_2O_{11}$ over 580°C, which exhibits a high oxide ion conduction **[1, 2]**. The substitution of vanadium in the parent compound $Bi_4V_2O_{11}$ stabilizes the best conductive γ- $Bi_4V_2O_{11}$ form at room temperature. Generally, compounds with tetragonal symmetry, and which stabilized at low temperature, can have a γ' form as a result of the partial ordering of oxygen vacancies in the γ form. There is no considerable structural difference between γ and γ' forms. However, the γ' form is less conductive than the former. Solid solutions derived from $Bi_4V_2O_{11}$ by partial substitution of vanadium with a large variety of metal ions of different sizes and valence states, possess a good oxide anion conductivity **[3-14]**. These materials are known as BIMEVOX where ME is the dopant metal **[3].** Generally, the best conductivity is obtained by substituting 10% of V^{5+} ions in $Bi_4V_2O_{11}$**[15]**. These compounds are solid electrolytes used in many promising applications including oxygen sensors, oxygen pumps, and fuel cells. The presence of vacancies, the stereoactivity of bismuth lone pair, and disorder in the anionic sublattice, are at the origin of the high conductivity of these compounds **[3].**

Double-substituted $Bi_4V_{1.8}M_{0.2-x}M'_xO_{11\pm x}$ solid solutions have been previously reported **[16-19]**. They were prepared in order to induce some additional disorder in the metal's site and

then improve the conductivity. In a previous study, we have reported some data about double substitution of V^{5+} by (Cu^{2+}, Nb^{5+}) **[20]** and by (Cu^{2+}, Co^{2+}) **[21].** More recently, we have investigated the structural and ionic conductivity changes, when vanadium is doubly substituted by (Cu^{2+}, Al^{3+}) in $Bi_4V_{1.8}Cu_{0.2-y}Al_yO_{10.7+y/2}$ compounds **[22].** We have shown an improvement in conductivity in spite of the decrease of the vacancies number in the anionic sublattice when y increases. This reflects the significant effect of the double substitution in these materials ($\sigma_{600\ C}$=4.16 × 10^{-2} S.$cm^{-1}$for $Bi_4V_{1.8}Cu_{0.2}O_{10.7}$ compound **[18]** and $\sigma_{600\ C}$=7.24 × 10^{-2} S.cm^{-1} for $Bi_4V_{1.8}Cu_{0.15}Al_{0.05}O_{10.725}$ compound **[22]**). In this context, it would be interesting to explore a larger domain of stability of the tetragonal phase for amounts of substitution of vanadium x≥0.20. Thus, we have been interested in the compounds with the formula $Bi_4V_{2-x}Cu_{x/2}Al_{x/2}O_{11-5x/4}$. Otherwise, continuing to increase the amount of doping was attempted with other dopants all over the range of occurrence of $Bi_4V_{2-x}M_{x/2}M'_{x/2}O_{11-\delta}$ solid solutions **[16, 23-25].**

The purpose of the present work is to investigate the effect of the double-substitution of vanadium by (Cu^{2+}, Al^{3+}) on structural properties and ionic conductivity of $Bi_4V_{2-x}Cu_{x/2}Al_{x/2}O_{11-5x/4}$ compounds with identical quantitative compositions of Cu^{2+} and Al^{3+} for $0.1 \leq x \leq 0.6$. The chemical formulas used ($Bi_4V_{2-x}Cu_{x/2}Al_{x/2}O_{11-5x/4}$) indicates the theoretical compositions where vanadium is exclusively in the +5 oxidation state.

2. Experimental procedure

Samples of $Bi_4V_{2-x}Cu_{x/2}Al_{x/2}O_{11-5x/4}$ powders were prepared based on the conventional solid-state reaction. Accurately weighted stoichiometric quantities of oxide reagents powders (Bi_2O_3, V_2O_5 and CuO) were homogenized, and then ground in an agate mortar. The obtained blends were heated in a platinum crucible at 840 °C in the open air for 24h. They were then slowly cooled to room temperature. Pellets (diameter of 13 mm, and ~ 2 mm thick) were prepared using ground powders sieved at 50-µm and pressed using an uniaxial hand pressing (0.5 ton/cm^2). The obtained pellets were sintered in the open air at temperature T_s and then quenched at room temperature. The apparent densities were determined by measuring the mass and size of the sintered pellets. The relative densities were estimated by dividing the apparent densities by theoretical ones, which were calculated using unit cell parameters.

The powder samples were characterized by X-Ray Diffraction using an XPERT MPD Philips diffractometer with Cu *K*α radiation. The patterns were recorded between 5° and 70° (2θ), with a step of 0.02° (2θ) and counting time of 4 s per step.

The variation of the unit-cell parameters and the cell volume were obtained using the indexing program Dicvol 04 **[26**].

Differential thermal and thermogravimetric analyses (DTA-DTG) were carried out on samples at increasing temperature from 25°C to 700°C, using an AT 1500 Analyzer at a heating rate of 10 °C.min^{-1}.

The infrared study was performed on KBr pellets. Each sample was mixed with dried potassium bromide (KBr) at a sample to KBr amount ratio of 2: 200 mg. The mixture was then compressed under vacuum. The pellets were analyzed over a frequency range of 4000 to 400 cm^{-1} using a Bruker Vertex 70 FTIR spectrometer equipped with a DTGS detector and OPUS 6.5 software; 128 sweeps with a resolution of 2 cm^{-1} were performed.

Ionic-conductivity measurements were performed by Electrochemical Impedance Spectroscopy (EIS) at frequencies ranging from 0.01 to 1 MHz using a Solartron SI 1260 Impedance Gain Phase Analyzer. The amplitude of the AC signal applied across the sample was 50 mV. Measurements were performed on sintered pellets (relative density ≈ 85%) under steady state conditions. Pt electrodes were deposited on both flat surfaces of the pellets. Pellets were first heated to 830 °C with a 15 h-dwell time. For each sample, the impedance measurements were made under dry air from 120 to 700 °C, on isothermal plateau of 30 mn. The experimental impedance diagrams were simulated by equivalent circuits composed of resistances and Constant Phase Elements (CPE). The values of circuit parameters were determined by non-linear least-square fitting using the Z.View software (Scribner Associates).

3. Results and discussion

3.1. Solid solutions' characterization

The XRD analysis, at room temperature of powders shows that the $Bi_4V_{2-x}Cu_{x/2}Al_{x/2}O_{11-5x/4}$ solid solution is obtained as a single phase in the range of composition $0.1 \leq x \leq 0.6$ (where x is the substitution ratio). The X-ray diffraction patterns **(**Fig.1) show no secondary phase formation.

The solid solution disappear for $x > 0.6$ since a secondary phase indexed as $Bi_8V_2O_{17}$ is detected beside the γ-$Bi_4V_2O_{11}$ phase (Fig.1). $Bi_8V_2O_{17}$ is in fact commonly observed as a secondary phase in the synthesis of BIMEVOX compounds **[27-29].**

The XRD analysis at room temperature, of the solid solution with x=0.1, shows a superstructure peak at ~ 24°C, which is related to the monoclinic α-form of $Bi_4V_2O_{11}$ with C2/m space group. With increasing x, the coalescence of the doublet diffraction peak at about 32° into (110) singlet **[8, 22, 30]**, reveals that the tetragonal γ or γ' form of $Bi_4V_2O_{11}$ is stabilized over the whole composition range $0.2 \leq x \leq 0.6$.

The variation of the unit-cell parameters and the cell volume as a function of x is shown in Fig.2**.** The $Bi_4V_2O_{11}$ polymorphs can be described in a mean orthorhombic unit cell with a_m=5.5 Å, b_m=5.6 Å and c_m=15.3 Å **[31**]. Thus, values of the unit cell parameters are multiplied by $\sqrt{2}$ for compounds with tetragonal symmetry. For compounds with monoclinic symmetry, lattice parameters are related to the orthorhombic unit cell through the relations: $a=c_m/3$, $b=a_m$ and $c=b_m$.

In the γ-form's composition range, the **c** parameters and the volume increase when x increases, while the **a** parameter shows no variation. The increase of the **c** parameter ($\Delta\mathbf{c}/\mathbf{c} \approx 0.58\%$) can be explained by the effective ionic radius difference especially of the Cu^{2+} and V^{5+} $r_i(Cu^{2+})$ = 0,73Å, $r_i(V^{5+})$ = 0,54Å and $r_i(Al^{3+})$ = 0.53Å) **[32].** The stability of the **a** parameter and the more pronounced increase of the **c** parameter, at least for $x < 0.4$, can be due to the distribution of oxygen vacancies in the equatorial positions rather than those at the summit positions. However, the less pronounced increase of the **c** parameter for $x \geq 0.4$ may be attributed to the oxygen vacancies, which begin to be located at apical positions. The sample with x = 0.1, compared with the parent compound, exhibits a decrease of the volume cell due to cell shrinkage in (a, b) plan.

For x = 0.1, the XRD analysis result is confirmed by the endothermic peak detected around 470°C on the DTA thermogram for this material (Fig.3.a). The presence of this peak can be assigned to the α to γ transition. In accordance with XRD results, the DTA curve of the compound with x = 0.5 (Fig.3.b) shows an endothermic and a peak around 540°C, which can be attributed to a transition from ordered γ' to disordered γ form. On the other hand, the DTA diagram of the x = 0.3 sample (Fig.3.c) does not exhibit any peaks, which indicates the stabilization of the γ form at room temperature.

The FT-IR spectra of $Bi_4V_{2-x}Al_{x/2}Cu_{x/2}O_{11-\delta}$ in the range of 4000 to 400 cm^{-1} of the samples with different compositions ($0.1 \leq x\ 0.6$) are illustrated in the figure 4. All the spectra show a water band at 1638 cm^{-1} and 3245 cm^{-1} along with a broad band around 3450 cm^{-1} **[33]** due to adsorbed water in the powdered samples required for making pellets.

FT-IR spectra of all samples show three well-known bands observed in the band ranges: 510-520; 700-830 and 1000-1040 cm^{-1}. The band around 515-520 cm^{-1} is assigned mainly to the stretching vibrations of Bi–O bond in the BiO_6 octahedral units **[34, 35]**. The band observed in this area at 520 cm^{-1} was also assigned to the stretching vibrations of Bi–O bonds in distorted BiO_6 octahedral units over which longitudinal stretching mode of $V–O_A$ is superimposed **[36, 37]** (O_A : is oxygen in apical position in perovskite-like sheets $(VO_{3.5}\square_{0.5})^{2-}$). The bands around 738 and 818 cm^{-1} are due to the stretching vibration of $V–O_A$ **[38, 39]**. A strong band at 1032 cm^{-1} is attributed to the vibration of isolated V=O vanadyl groups in the VO_5 trigonal bipyramidal unit **[40, 41].** The FTIR spectra show, depending on the composition, that some bands move to low or high frequencies, while other bands disappear completely from the spectrum.

In the high-frequency region, the band attributed to the antisymmetric vibration shifts progressively from 810 to 818 cm^{-1} as x increases, while the wave numbers attributed to the symmetrical vibration, which appears at 738 cm^{-1}, does not change. The opposite effect was observed during the substitution of vanadium by Hf where a decrease of the asymmetric mode wavenumbers is observed **[42]**. Accordingly, the cation size has an effect on the band shifts direction in the infrared spectrum. In contrast, the band of the parent product spectrum, situated at about 500 cm^{-1}, shifts towards the high frequencies up to x = 0.3, then slides towards the low frequencies for x > 0.3. The same band shift was observed when Bi was substituted by Pb in the BiO_6 units. This shift was explained by the perturbation of the Bi-O units by Pb **[13]**, which also affects $V-O_A$ units. In this case, this band is attributed to the stretching vibration of the Bi-O groups located in distorted octahedral units **[13, 43-44]**. Our results confirm that the $V-O_A$ bond is also influenced by the Al/V substitution in the VO_6 units. As a result, the vibrations in the VO_6 units do not occur independently of the other units (BiO). The analysis of FTIR spectra cannot be done according to the approximation of "isolated" units as in the case of perovskite structures **[45, 46]**.

Moreover, compared to the spectrum of the starting sample (x = 0), we find that the bands at 768 615, and 425 cm^{-1} disappear completely from the IR spectrum at the beginning of the substitution (x=0.1) Fig.5. This can be attributed to the interdiction of vibration modes following a change in the local symmetry. This hypothesis is justified by the measurements of the cell parameters (Fig.2). In fact, for x = 0.1, we observe that the parameter **b** decreases while the parameter **a** increases. Such modifications of **a** and **b** parameters lead to a decrease in the cell volume although the parameter **c** increases. This decrease in volume can be explained by significant contractions occurring in the (a, b) plan and which are not compensated by the

increase of the parameter **c**. For x = 0.2 and x = 0.3, we note the appearance of two bands towards 450 and 425 cm^{-1}, which disappear for x > 0.4. These spectroscopic modifications reveal that the degree of substitution causes changes in spectroscopic activities by degeneration or by interdiction of the activity of some vibration modes.

3.2. Electrical conductivity

Measurements were performed on sintered pellets in the open air at Ts = 830°C for 15 h. The samples analyzed show relative high densities around 85% and a shrinkage, which fluctuates around 10%.

Typical Nyquist diagrams for the $Bi_4V_{1.70}Cu_{0.15}Al_{0.15}O_{10.625}$ (x=0.3) system at different temperatures are shown in Fig.6. Generally, the oxide-ion conductors exhibit two semicircular contributions. However, the impedance diagrams for $Bi_4V_{1.70}Cu_{0.15}Al_{0.15}O_{10.625}$ are characterized by a single arc at higher frequencies that reflects both grain-interior and grain-boundary effects. The straight lines observed at low frequencies correspond to the electrode polarization behavior.

Fig.7 illustrates the Arrhenius plots of the $Bi_4V_{2-x}Cu_{x/2}Al_{x/2}O_{11-5x/4}$ ionic conductivity over the temperature range of 250°C to 700°C. For a sample with x = 0.1, we notice a straight line with low activation energy at high temperatures. With a decrease in temperature, two drops in conductivity diagrams occur at around 500°C and 370°C. These discontinuities can be assigned to the $\alpha \leftrightarrow \beta \leftrightarrow \gamma$ structural transitions. DTA analysis shows only one transition, which can be explained by a direct passage from α to the γ form. For the tetragonal phases with $0.2 \leq x \leq 0.6$, a flexion in the conductivity curve is detected for all samples in the temperature range of 350°C–450°C due to a change in the slope. This behavior is characteristic of $\gamma' \leftrightarrow \gamma$ phase transition, and can be related to the fast kinetic of this transition, which implies a slight vacancy ordering. However, this transition is not observed in the DTA curve for x=0.3 sample (Fig.3-c**)**. In the Arrhenius plots (Fig.7), the $\gamma' \leftrightarrow \gamma$ phase transition can be depicted by a change in the activation energy. The same result was observed in the $Bi_4Ba_xV_{2-x}O_{11-\delta}$ solid solution **[47]**. In addition, we can note that the sample with x = 0.3 composition, exhibits the smallest variation of activation energy between the high and low-temperature ranges (Table 1).

In Fig.8, we report the trend of the electrical conductivity as a function of the composition for the tetragonal phases. Both high-temperature $\sigma_{600\ C}$ and low-temperature $\sigma_{300\ C}$ conductivities decrease with the composition which, is the typical tendency of the BIMEVOX compounds **[47-49]**. This decrease in conductivity can be imputed to the ordering of oxygen vacancies **[50-52].** For x > 0.3, electrical conductivity becomes less sensitive to the composition.

Fig. 9 shows the variation of the activation energy as a function of the amount of substitution. The sample with x = 0.1 has higher activation energies than the parent compound $Bi_4V_2O_{11}$ (Table 1). This may be related to changes in local symmetry as claimed from both XRD results that indicate a decrease in cell volume and the activity changes in the FT-IR spectrum after substitution. At high temperature, samples with $x \leq 0.3$ show activation energies in the range of 0.26–0.42 eV, as generally obtained for γ-type phases **[3, 19-22]**. However, the activation energy values obtained for x > 0.3 are unusually higher. Fig.9 shows also a different behavior for the x = 0.4 and x = 0.5 samples compared to the x = 0.2 and x = 0.3 samples. The high activation energies in the case of these compounds can be explained by the creation of oxygen vacancies in the apical positions leading to a long-term ion exchange in the vanadate layers. This change in the vacancy positions can be at the origin of those modifications. This is

confirmed by the variation of the full width at half maximum of the band ($\Delta\nu_{1/2}$) situated around 520 cm^{-1} vs. the composition. Surprisingly, for $0.2 \leq x \leq 0.4$, the shape of the curve (Fig 10) is the same as those observed in the variation of activation energies (Fig. 8) and those of the conductivity (Fig. 9). If we assume that this band is attributed to the Bi-O_A / V-O_A vibration, the position disorder of the oxygen, which is certainly variable, must contribute to the enlargement of the bands. The change of the full width at half maximum of the band situated around 520 cm^{-1} in the FTIR spectra confirms that the oxygen (O_A) environment is altered during the substitution. So, the width at the half height of the band occurred around 520 cm^{-1} informs about disorder surrounding Bi-O_A / V-O_A bands.

4. Conclusion

The solid solution of BIMEVOX family (Me: Cu, Al) was prepared as a single phase. The compositions $Bi_4V_{2-x}Cu_{x/2}Al_{x/2}O_{11-5x/4}$ ($0.2 \leq x \leq 0.6$) were found to keep a tetragonal γ structure at room temperature. Impedance spectroscopy study revealed that the prepared solid solution has enough high values of electrical conductivity. Changes in conductivity and activation energy values are strongly related to those in the local symmetry. The variations in cell parameters, band profiles and FTIR activity of vibration during substitutions may be attributed to the distribution of oxygen vacancies. This undoubtedly causes disruption of the local symmetry at the vanadate layers.

References

[1] A.A. Bush, Yu.N. Venevtsev, Rus.J.Inorg., 35 (5) (1986) 767.
[2] F. Abraham, M.F. Debreuille-Gresse, G. Mairesse, G. Nowogrocki, Solid State Ionics, 28-30 (1988), 529.
[3] F. Abraham, J.C. Boivin, G. Mairesse, G. Nowogrocki, Solid State Ionics, 40-41 (1990), 934.
[4] J.B. Goodenough, A. Manthiram, M. Paranthaman, Y.S. Zhen, Mater. Sci. Eng. B, 12 (1992) 357.
[5] R. Essalim, B. Tanouti, J.P. Bonnet, J.M. Réau, Mater. Lett., 13(1992) 386.
[6] V. Sharma, A.K. Shukla, J. Goplakrishnan, Solid State Ionics, 58 (1992) 359
[7] A. Watanabe, K. Das, J. Solid State Chem., 163 (2002) 224.
[8] E.S. Buyanova, M.V. Morozovz, Ju. V. Emelyanova, S.A. Petrova, R.G., Zakharov, N.V. Tarakina, V.M. Zhukovskiy, Solid State Ionics, 243 (2013) 8.
[9] M. Roy, S. Sahu, S.K. Barbar, S. Jangid, Adv. Mat. Lett., 5(3) (2014) 122.
[10] M. Alga, A. Ammar, R. Essalim, F. Mauvy, R. Decourt, B. Tanouti, Solid State Sciences, 7 (2005) 1173.
[11] M. Alga, A. Ammar, M. Wahbi, B. Tanouti, J.C. Grenier, J.M. Réau, J. of Alloys Compounds, 256 (1997) 234.
[12] J. Yan, M. Greenblatt, Solid State Ionics, 81 (1995) 225.
[13] R. Kaur, S. Thakur, K. Singh, Physica B, 440 (2014) 78.
[14] M. Roy, S. Sahu, J. Integrated Science & Technology 2 (2) (2014) 49.
[15] G. Mairesse, B. Scrosati, A. Magishis, C.M. Mari, G. Mariotto (Eds.), Fast Ion Transport in Solids, Kluwer, Dordrecht, 1993, p. 271.
[16] M.V. Morozova, E.S. Buyanova, Yu.V.Emelyanova, V.M. Zhukovsky, S.A., Petrova,R.G. Zakharov, N.V. Tarakina, Solid State Ionics 201 (2011) 27.
[17] R.N. Vannier, G. Mairesse, F. Abraham, G. Nowogrocki. Solid State Ionics 70/71 (1994) 248.

[18] M.H. Paydar, A.M. Hadian, G. Fafilek, J. Eur. Ceram. Soc. 21 (2001) 1821.
[19] S.Beg and N.S. Salami, J. Alloys Compounds 586 (2014) 302.
[20] M. Alga, A. Ammar, B. Tanouti, A. Outzourhit, F. Mauvy, R. Decourt. J. of Solid State Chem. 178 (2005) 2873.
[21] M. Alga, A. Ammar, R. Essalim,B. Tanouti, A. Outzourhit, F. Mauvy, R. Decourt. Ionics 11 (2005) 81.
[22] R.Essalim, A.Ammar, B.Tanouti and F.Mauvy. J. Solid State Chem. 240(2016)122.
[23] S. Beg, S. Haneef, J. Phase Transition, 88(11) (2015) 1074
[24] M.V. Morozova, E.S. Buyanova, Yu.V. Emel'yanova, V.M. Zhukovskiy and S.A. Petrova, Solid State Ionics 192 (2011) 153.
[25] E.V. Velichko, Z.A. Mikhailovskoya, M.V. Morozova, E.S. Buyanova, Yu.V. Emel'yanova, S.A. Petrova and V.M. Zhukovskiy, Russ. J. Electrochem. 47(5) (2011) 563.
[26] A. Boultif, D. Louer, J. Appl. Cryst. 37 (2004) 724-731
[30]. Y.K. Taninouchi, T. Uda, T. Ichitsubo, Solid State Ionics 181 (2010) 719
[31] G.N. Subbanna, I Ganapathi, Bull. Mater. Sci. 9 (1987) 29
[32] R.D. Shannon, Acta Crystallogr, A 32 (1976) 751.
[33] I.I. Stravoitov, S.A.Selifonov, M.Yu Nefedova and V.M. Adanin, Biol. Bull. Acad. Sci. USSR, 15(1-3)(1988) 38.
[34] R. Punia, R.S. Kundu, J. Hooda, S. Dhankhar, S. Dahiya, N. Kishore, J. Appl. Phys. 110 (2011) 033527.
[35] P. , T. Thongtem, A. Phuruangrat, S. Thongtem, J. Super- lattices Microstruct. 54 (2013) 71.
[36] S.S. Rojas, J.E. De Souza, M.R.B. Andreeta, A.C. Hernandes, J. Non-Cryst. Solids 356 (2010) 2942.
[37] F.H. ElBatal, M.A. Marzouk, A.M. Abdelghany, J. Non-Cryst. Solids 357 (2011) 1027.
[38] A.A. El-Moneim, Mater. Chem. Phys. 73 (2002) 318. [38] V. Dimitrov, A. Yanko Dimitriev, J. Non-Cryst. Solids 180 (1994) 51.
[39] V. Dimitrov, A. Yanko Dimitriev, J. Non-Cryst. Solids 180 (1994) 51.
[40] D. Manara, A. Grandjean, O. Pinet, J.L. Dussossoy, D.R. Neuville, J. Non-Cryst. Solids 353 (2007) 12.
[41] S. Rada, E. Culea, V. Rus, M. Pica, M. Culea, J. Mater. Sci. 43 (2008) 3713.
[42] S. Beg, N.A.S. Al-Areqi, A.A. Ahlam, J. Alloys Compounds 479 (2009) 107.
[43] S.S. Rojas, J.E. De Souza, M.R.B. Andreeta, A.C. Hermandes, J. Non-Cryst Solids 356 (2010) 2942.
[44] F.H. Elbatal, M.A. Marzouk, A.M. Abdelghany, Non-Cryst Solids 357 (2011) 1027.
[45] A. E. Lavat, E. J. Baran, Vibrat. Spectr. 32 (2003) 167
[46] Araceli E. Lavat, Enrique J. Baran J. of alloys. And Compounds 460 (2008) 152
[47] S. Gupta, K. Singh, Solid State Ionics 278 (2015) 233
[48] O. Joubert, M. Ganne, R.N. Vannier, G. Mairesse, Solide State Ionics 83 (1996) 199.
[49] F. Krok, I. Abraham, D.G. Bangobango, W. Bogusz, J.A.G. Nelstrop, Solid State Ionics 86-88 (1996) 261.
[50] Yu.V. Emel'yanova, Z.V. Salimgareeva, E.S. Buyanova, V.M. Zhukovskiy, Inorg. Mater. 41 (10) (2005) 1107.
[51] I. Abraham, F.Krok, J. Mater. Chem.12 (2002) 2260.
[52] I. Abraham, F.Krok, M. Malys, W. Wrobel, Solid State Ionics 176.

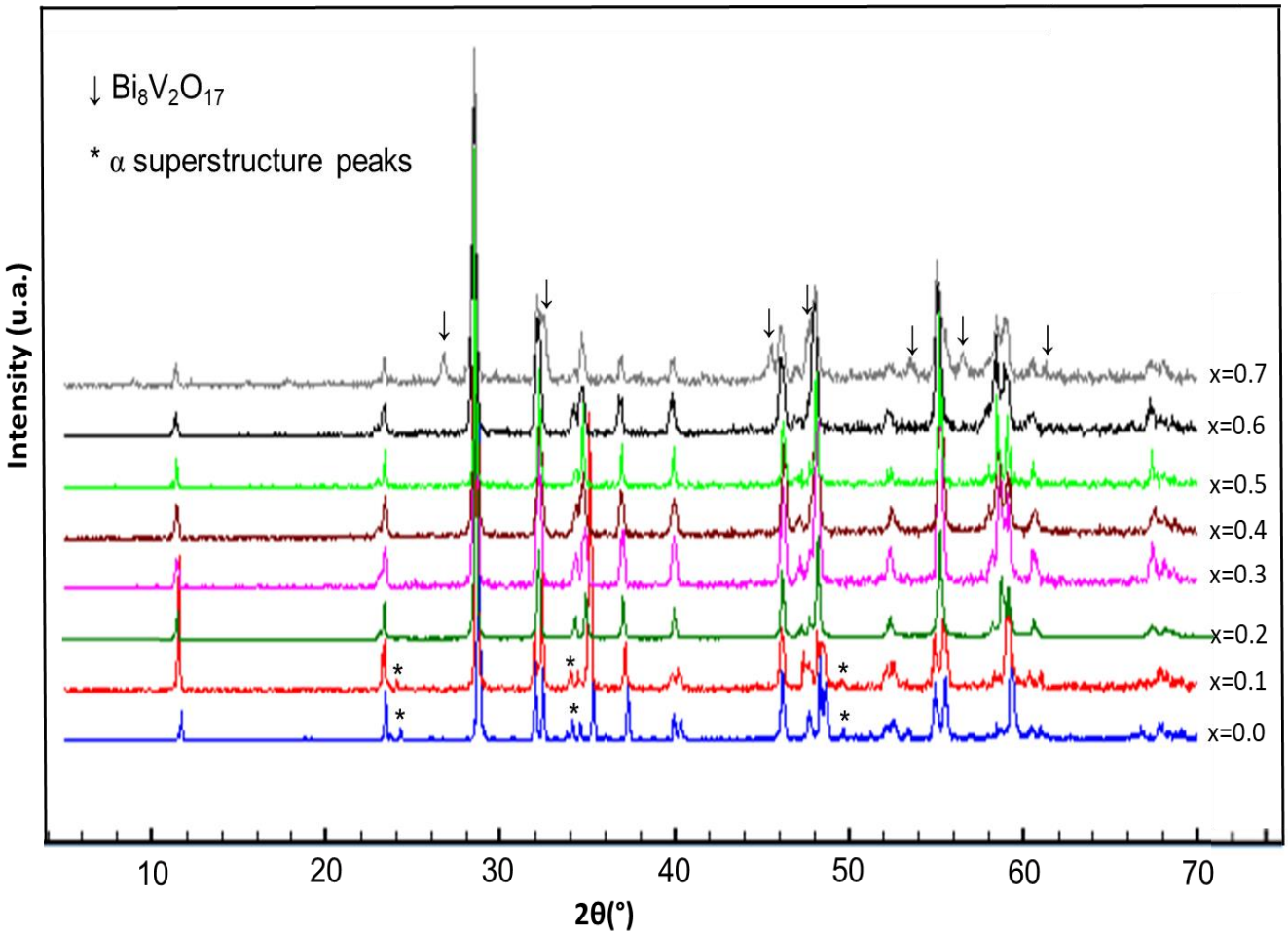

Fig.1. X-ray diffraction patterns of $Bi_4V_{2-x}Cu_{x/2}Al_{x/2}O_{11-5x/4}$.

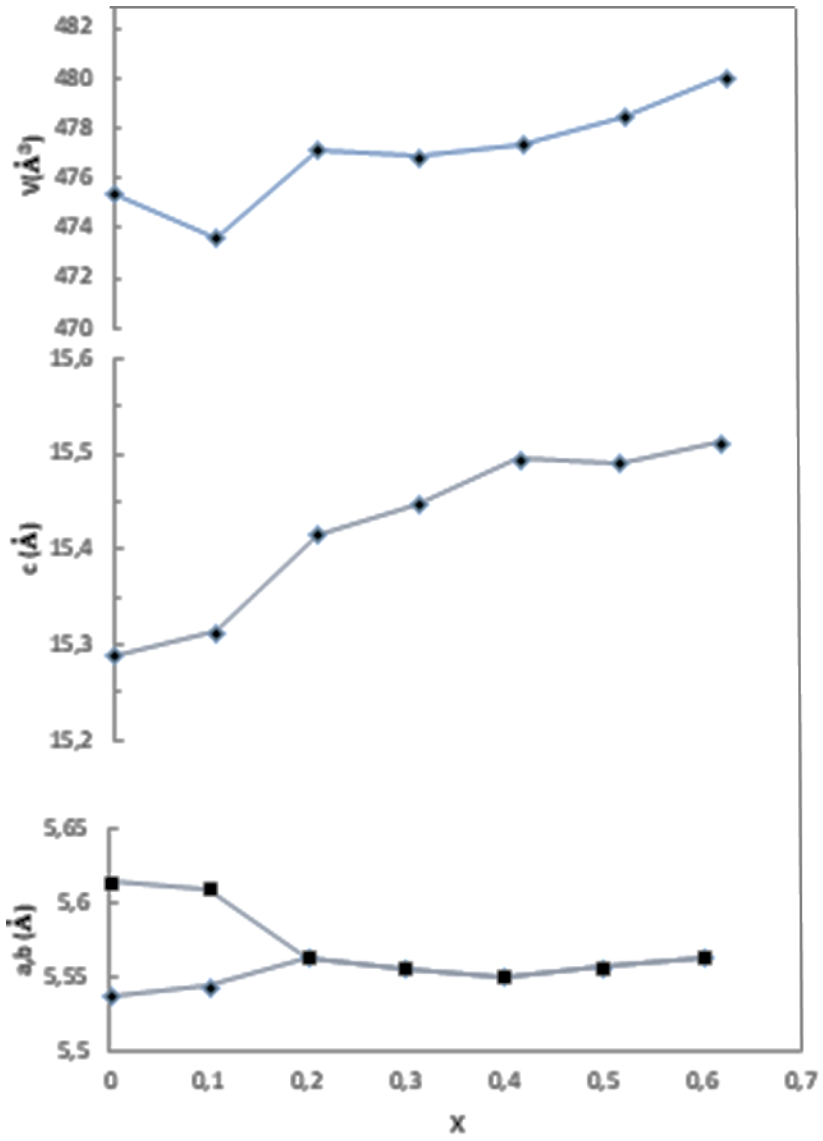

Fig.2. Evolution with x of the lattice paramaters and the cell volume of $Bi_4V_{2-x}Cu_{x/2}Al_{x/2}O_{11-5x/4}$ *solide solution.*

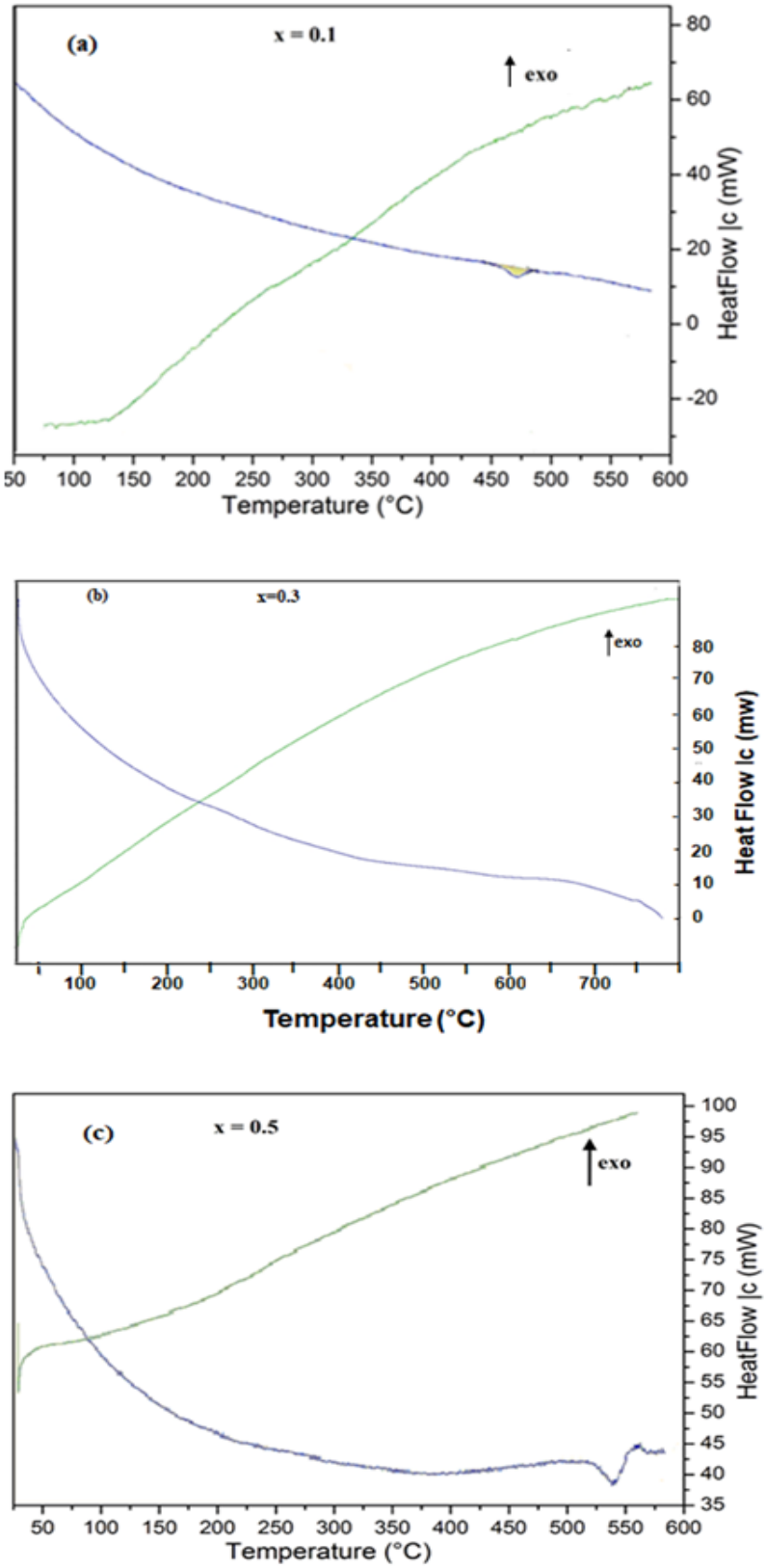

Fig.3. DTA curves (blue) of $Bi_4V_{2-x}Cu_{x/2}Al_{x/2}O_{11-5x/4}$ *solid solution.*

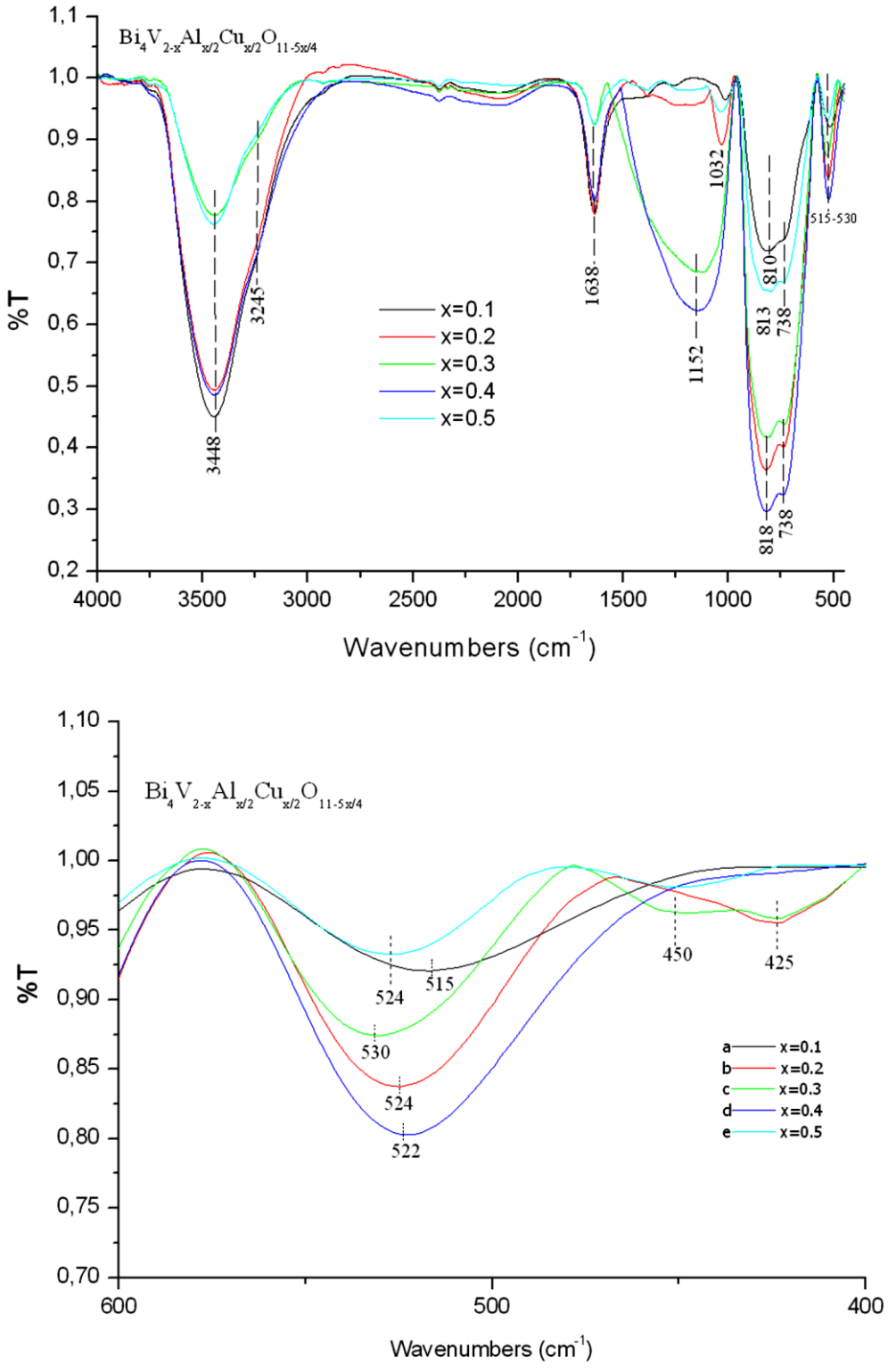

Fig.4. Infrared spectrum of $Bi_4V_{2-x}Cu_{x/2}Al_{x/2}O_{11-5x/4}$compounds.

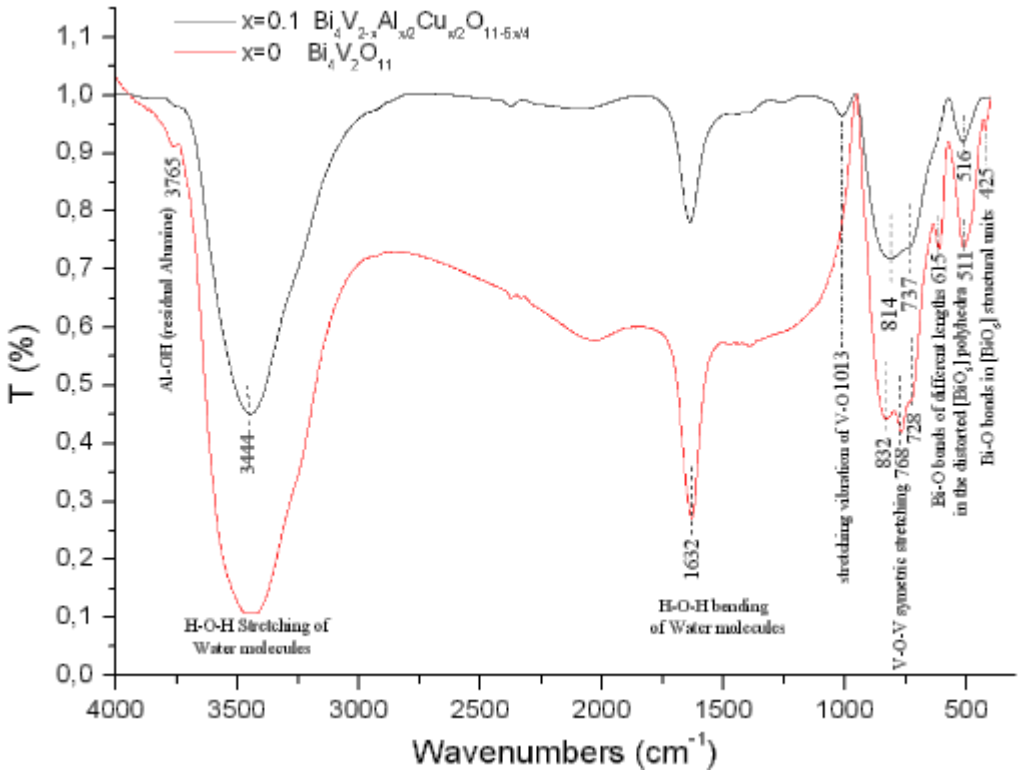

Fig.5. Infrared spectrum of $Bi_4V_2O_{11}$ and $Bi_4V_{1.9}Cu_{0.05}Al_{0.05}O_{10.875}$compounds

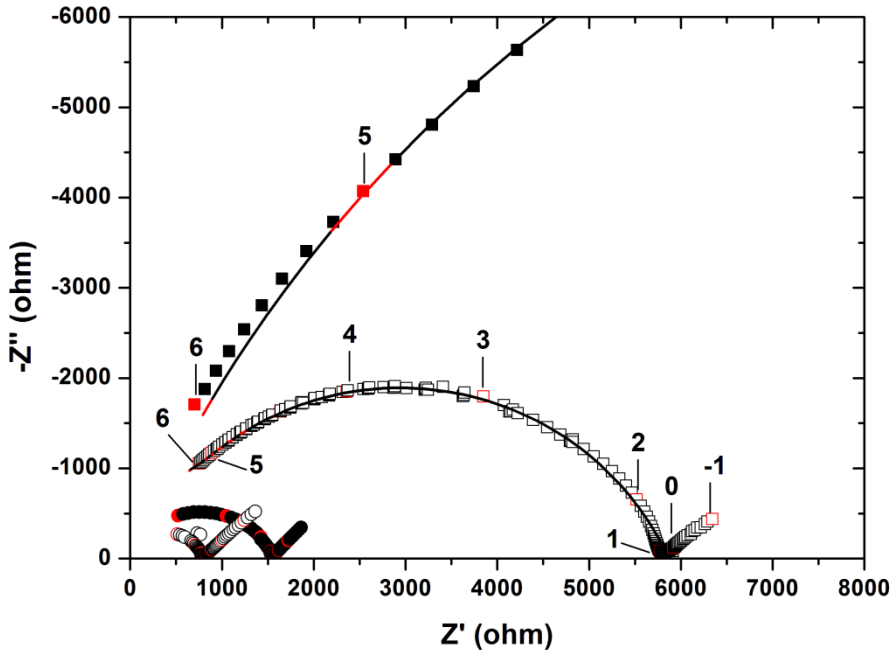

Fig.6. Typical Nyquist diagrams for $Bi_4V_{1.7}Cu_{0.15}Al_{0.15}O_{10.625}$(x=0.3) at T=153°C (full square), at T=201°C (empty square) at T=252°C (full circle) and at T=304°C (empty circle) under air. The numbers inside are the logarithm of frequencies.

Fig.7.Arrhenius plots of the electrical conductivity of the $Bi_4V_{2-x}Cu_{x/2}Al_{x/2}O_{10.7-5x/4}$ *compounds.*

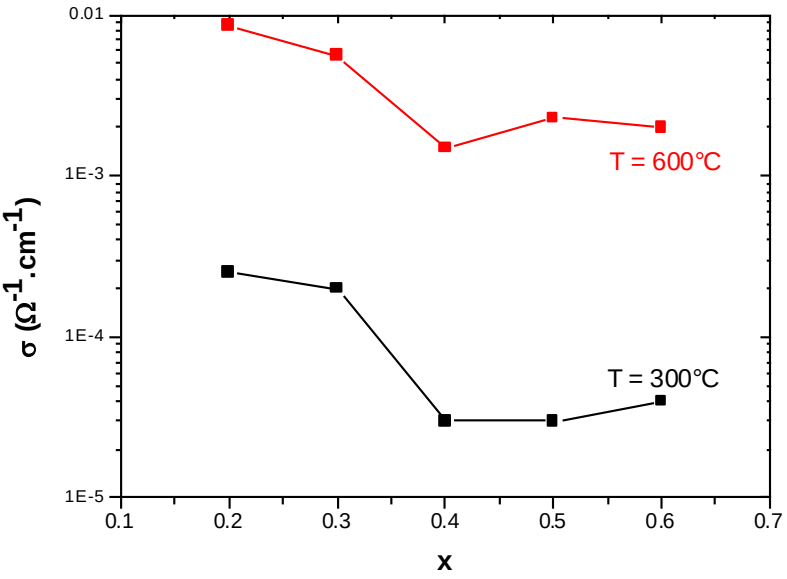

Fig.8.Variation of the electrical conductivity as a function of composition for tetragonal phases.

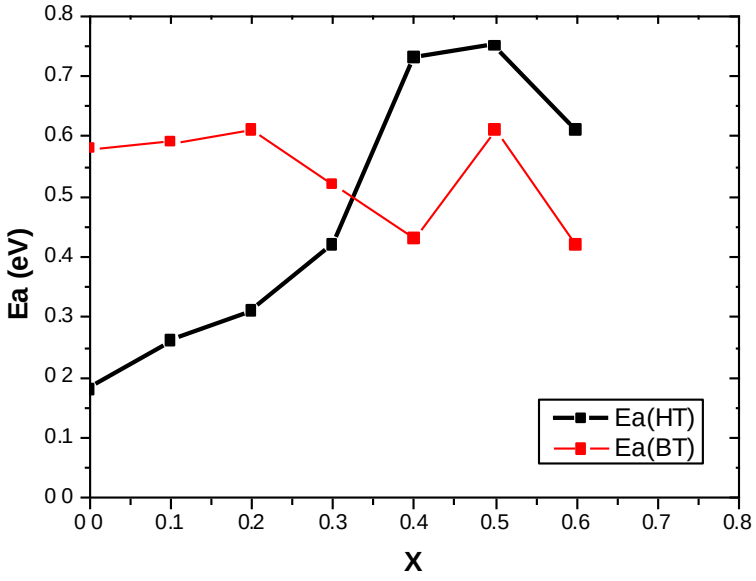

Fig.9.Variation of the activation energy as a function of composition for $Bi_4V_{2-x}Cu_{x/2}Al_{x/2}O_{10.7-5x/4}$.

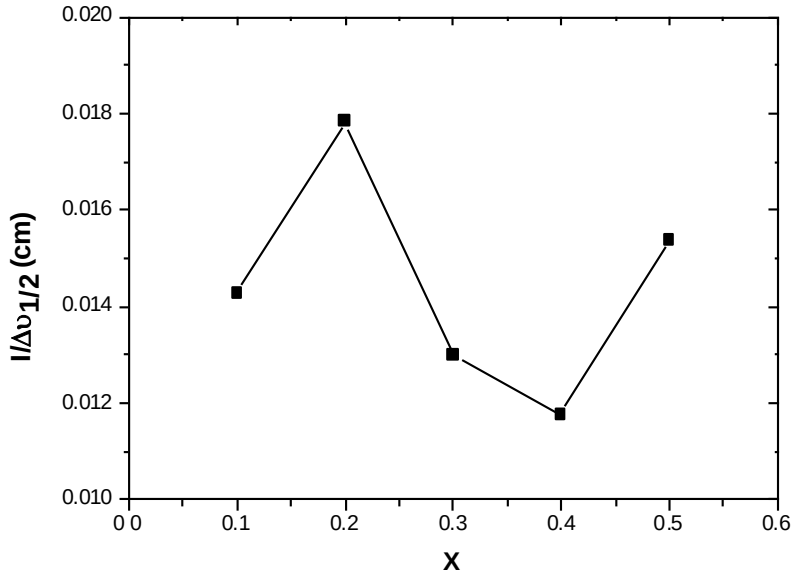

Fig.10: FTIR spectra-Variation of the width at half-height of the band situated around 500 cm^{-1} as a function of composition.

Table1. Conductivity and activation energy of $Bi_4V_{2-x}Cu_{x/2}Al_{x/2}O_{11-5x/4}$ compounds.

x	Composition	$\sigma_{300\ C}$ ($S.cm^{-1}$)	$\sigma_{600\ C}$ ($S.cm^{-1}$)	E_{aHT} (eV)	E_{aMT}(eV)	E_{aBT} (eV)	Ref.
0.0	$Bi_4V_2O_{11}$	7.5×10^{-5}	10^{-1}	0.19	1.01	0.58	**[41]**
0.1	$Bi_4V_{1.9}Cu_{0.05}Al_{0.05}O_{10.875}$	2.0×10^{-7}	7.9×10^{-3}	0.26	1.82	0.59	This work
0.2	$Bi_4V_{1.8}Cu_{0.1}Al_{0.1}O_{10.75}$	2.5×10^{-4}	8.6×10^{-3}	0.31	-	0.61	This work
0.3	$Bi_4V_{1.7}Cu_{0.15}Al_{0.15}O_{10.625}$	2.0×10^{-4}	5.6×10^{-3}	0.42	-	0.52	This work
0.4	$Bi_4V_{1.6}Cu_{0.2}Al_{0.2}O_{10.5}$	3.0×10^{-5}	1.5×10^{-3}	0.73	-	0.40	This work
0.5	$Bi_4V_{1.5}Cu_{0.25}Al_{0.25}O_{10.375}$	1.4×10^{-5}	2.3×10^{-3}	0.75	-	0.61	This work
0.6	$Bi_4V_{1.4}Cu_{0.3}Al_{0.3}O_{10.25}$	4.0×10^{-5}	2.0×10^{-3}	0.61	-	0.42	This work